THERMAL INFLUENCE OF NON-UNIFORM INLET FLOW CONDITIONS FOR A COMMERCIAL PLATE FIN HEAT EXCHANGER

De Schampheleire S.*, De Kerpel K., Ameel B., Huisseune H. and De Paepe M.
*Author for correspondence
Department of Flow, Heat and Combustion Mechanics,
University of Ghent, UGent,
Sint-Pietersnieuwstraat 41, 9000 Ghent,
Belgium,
E-mail: Sven.DeSchampheleire@ugent.be

ABSTRACT

In this study, a commercially available plate heat exchanger with wavy fins is experimentally characterized under uniform and three non-uniform flow conditions. The heat exchanger is 275 mm wide and 295 mm high and has a distance in-between the plates of 3 mm and the wavy fins are 11 mm high. Internally, the heat exchanger is finned with offset strip fins. Hot water at 55°C is sent through the plates and the waterside mass flow rate is kept high in order to minimize the internal thermal resistance. For the internal convection coefficient, a correlation from literature is used. The airside mass flow rate is varied by adjusting the fan speed. In case of uniform flow conditions, the frontal air velocity varies between 1.7 and 7.6 m/s. The airside velocity is measured over a nozzle and the uniformity of the wind tunnel is verified by hot wire measurements. Three non-uniformities are placed 10 cm upstream of the heat exchanger: the first one covers the right-hand side of the heat exchanger, the second one covers the top half of the heat exchanger and the last (and most severe) non-uniformity consists of a circular hole of 150 mm diameter in the middle of a plate. Only the third non-uniformity has a significant influence on the heat transfer rate: up to 25% higher for the external convective resistance in comparison with the uniform case.

INTRODUCTION

Current heat exchanger design is based on both numerical and experimental work. Due to the decreasing cost of computational power, more and more heat exchangers are designed using CFD (computational fluid dynamics). Academic studies based on CFD only cover a small part of the heat exchanger (e.g. one fin row), as the computational efforts to calculate a complete heat exchanger are too high [1]. Complementary experimental work is still necessary. Experimentally, the heat exchanger is typically seen as a 'black box', with two fluid flows entering and exiting the unit, this is the Wilson plot technique [2]. An intermediate model of these two is using a 'heat exchanger model' as pre-programmed in CFD software like Fluent (Ansys®). Using heat transfer data from experiments, the program automatically convert this data to a mass flow rate vs NTU curve (on cell level). This curve can then be used to calculate the heat transfer rate when e.g. the (air) flow is non-uniform. By doing so, there is only need for one measurement campaign.

NOMENCLATURE

A	[m²]	area
B, w	[m]	width
c_p	[J/kgK]	specific heat
h	[W/m²K]	convection coefficient
h, H	[m]	height
j	[-]	colburn j-factor
E	[-]	effectiveness
$\dot{m}$	[kg/s]	mass flow rate
$\dot{Q}$	[W]	heat transfer rate
v	[m/s]	velocity
R	[K/W]	thermal resistance
Re	[-]	Reynolds number
l	[m]	fin depth
S	[m]	fin spacing
St	[-]	Stanton number
t	[m]	fin thickness
T	[K]	temperature
UA	[W/K]	overall heat transfer coefficient

Greek symbols

ρ	[kg/m³]	density
μ	[kg/s/m]	dynamic viscosity
η	[-]	fin efficiency

Subscripts

water	waterside
in	inside
ext	external
air	airside
out	outside

Manufacturers are continuously searching for more compact heat exchangers. They are using more advanced fin designs and place the fan as close to the heat exchanger as possible. The placement of the heat exchanger (in narrow channels or close to a fan unit) results in non-uniform flow conditions at the inlet of the heat exchanger. To compensate for these flow conditions, manufacturers apply safety factors. If the effect of these non-uniformities can be predicted with more detail, the safety factors can be lowered and the unit can be built more compact.

Studies on non-uniform inlet airflow (and temperature) distributions are only very limited. Beiler and Kröger [3] investigated the effect on the thermal performance of two unmixed fluids in cross-flow air-cooled heat exchangers. They found a maximum effect on the overall performance of 2%. T'Joen et al. [4] studied different types of non-uniformities (resp. quadratic, linear and cubic air distribution profiles) on a heat exchanger with adapted inclined louvered fins. These authors observed a maximum effect on the global heat transfer coefficient U for the quadratic flow profile of 8% (the relative uncertainty on the data is 6.8%).

In this work, a commercial wavy-fin and flat tube heat exchanger will be studied experimentally.

STUDIED HEAT EXCHANGER

The studied heat exchanger is shown in Figure 1, where the flow direction inside the tubes is also indicated. Hot water enters the collector on the right from below, is pumped through 18 flat tubes and exits the heat exchanger at the top of the collector on the left. Air flows over the fin side of the heat exchanger.

An automatic air vent is installed on top of the heat exchanger to ensure a proper degassing of the water circuit. The heat exchanger has a height (h) of 295 mm, a width (w) of 275 mm and a flow depth of 62.5 mm. The flat tubes are internally finned with strip fins, while there are wavy fins at the airside. The offset-strip fins (see Figure 3) are 3 mm height and 7.5 mm width (per unit cell), the fin spacing (offset on the fins) is 1.5 mm. The wavy fins (see Figure 4) are 11 mm high, 5 mm width, 13 mm long (per unit cell) and the fin spacing is 2 mm.

TEST RIG
Air- and waterside

The experimental set-up consists of an open air wind tunnel and a closed hot water cycle (see Figure 2). A centrifugal fan (Ventomatic® - AEC 355) sucks air through a calibrated nozzle. The pressure drop over that nozzle is measured with a differential pressure drop transducer and used to calculate the airside mass flow rate according to the DIN standardization. The motor of the fan has a frequency controller. To obtain a highly uniform velocity profile, a diffuser section is used, followed by a settling chamber with a flow straightener and a double sinusoidal contraction section (see Figure 2). This contraction section is built specifically for the studied heat exchanger (275x295mm²). Before the heat exchanger is placed in the test section, the uniformity of the air velocity at the test section inlet is confirmed for air velocities between 2.4 m/s and

9.7 m/s with 2D hot-wire measurements. Airside velocity uniformity ($\frac{v_{max}-v_{min}}{\frac{v_{max}+v_{min}}{2}}$) is always better than 2.5% while the turbulent intensity was always smaller than 2%.
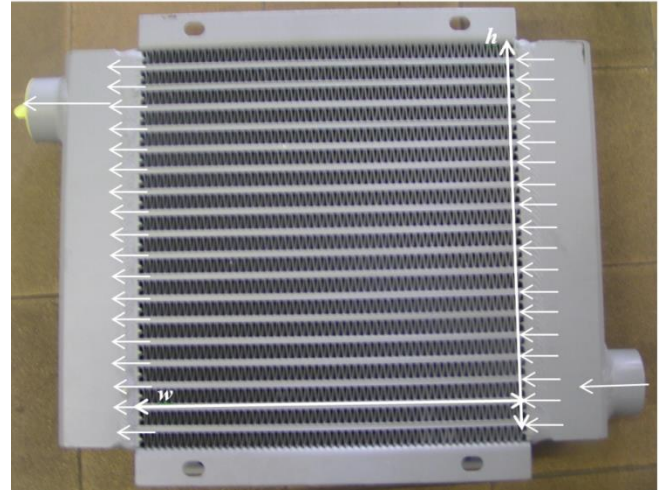
Figure 1 Picture of the studied commercial fin-and-tube heat exchanger

Four airside set points were taken for each flow condition. The air velocity at the test section inlet varies between 1.7 m/s and 7.62 m/s. Only for the last non-uniformity, the fan was not powerful enough to reach the highest air velocity target.

To provide heating, a closed hot water cycle is used. The heater has a maximum power of 9 kW(e). The water pump has a relay control and a motorized three way valve controls the waterside mass flow rate to the heat exchanger. The water mass flow rate through the heat exchanger is measured by a Coriolis mass flow meter (PROMASS 80-Endress+Hauser). The dashed rectangular zone in Figure 2 represents the test section and is completely insulated with Eurofloor® (0.023 W/mK) to minimize the heat loss to the environment.

The heater is controlled to send a certain amount of power to the water circuit. In steady-state operation conditions, this will result in a steady water inlet temperature. In this study the heater is controlled to an inlet water temperature of **55°C**. Steady-state is defined when the standard deviation of the average inlet water temperature varies less than 0.15°C over the last 150 measurements (sample rate 0.33Hz).

For all measurements, the waterside mass flow rate is set to a high and constant value of **600 kg/hr**. This ensures that the airside thermal resistance is dominant and the temperature difference on waterside is high enough (to measure it with an acceptable uncertainty). The external thermal resistance accounts for more than 75% of the overall thermal resistance. The airside mass flow rate is varied on **4 set points** (0.159,

0.346, 0.535 and 0.719 kg/s) by adjusting the frequency controller of the fan.

These experiments typically result in a $\dot{Q}_{avg} = \frac{\dot{Q}_{air}+\dot{Q}_{water}}{2}$, where the difference between $\dot{Q}_{air}$ and $\dot{Q}_{water}$ has to be as small as possible (according to ANSI/ASHRAE-33 standard: smaller than 5%), which indicates the accuracy of the test rig (minimal heat losses). However, for this specific heat exchanger, the measurement of $\dot{Q}_{air}$ is rather complex, as the exit angle of the air flow at the outlet of the heat exchanger is approximately 16° (corresponding the exit angle of the wavy fins – see Figure 4). This implies large non-uniformities in airside velocity at the outlet of the test section, which makes it difficult to measure an average air outlet temperature. An accurate measurement of the air outlet temperature implies that the local velocity and temperature is measured at a large number of points over the cross section of the test section exit. A mass flow average air outlet temperature can then be determined. Next, $\dot{Q}_{air}$ can be calculated and the difference between $\dot{Q}_{air}$ and $\dot{Q}_{water}$ can be determined (to check the heat balance). This is done for one velocity set point to verify the accuracy of the test rig (local velocity measurements were performed with a hotwire system). The heat balance closes within 3%. The results are however not reported here. The closed heat balance proves that there are no significant heat losses to the environment. That is why for the measurements $\dot{Q}_{air}$ is taken equal to $\dot{Q}_{water}$. The latter can be measured with smallest uncertainty. Measuring the temperature distribution over the test section outlet is than no longer needed. This greatly simplifies the measurement campaign. For all other results, basically five parameters ($\dot{m}_{water}$, $T_{water,in}$, $T_{water,out}$, $\dot{m}_{air}$ and $T_{air,in}$) are continuously logged.

Non-uniformities

For the first non-uniform flow condition, the Plexiglas® plate covers exactly half of the test section and is placed on the side of the hot water inlet, where the largest thermal effect is expected. The Plexiglas® plate has a thickness of 5 mm.

The second non-uniformity the upper half of the inlet is blocked with a Plexiglas® plate. The plate also has a thickness of 5 mm. There is no specific reason why the upper half is blocked: no thermal or hydraulic effect is expected.

The third and last non-uniformity consists of a hole of 150 mm diameter in the middle of the test section. The thickness of the Plexiglas® plate is again 5 mm. For this non-uniformity only 78.2% of the flow area is covered (instead of 50% for the two other non-uniformities).

Measurement accuracy

The air- and waterside mass flow rates can be measured accurately. The relative uncertainty on $\dot{m}_{air}$ is 1.5% or 3.5%, depending on the pressure drop transducer used. The relative uncertainty follows the Deutsches Institut für Normung (DIN) guidelines. The (relative) uncertainty on $\dot{m}_{water}$ varies on the absolute number of the mass flow rate according to the calibration done by the manufacturer. For this study and the selected mass flow rate, the uncertainty on $\dot{m}_{water}$ is taken as the quadratic sum of the absolute error (0.15% of the measured value) and twice the standard deviation ($\sqrt{(0.15\% \cdot measured\ value)^2 + (2\sigma)^2}$).
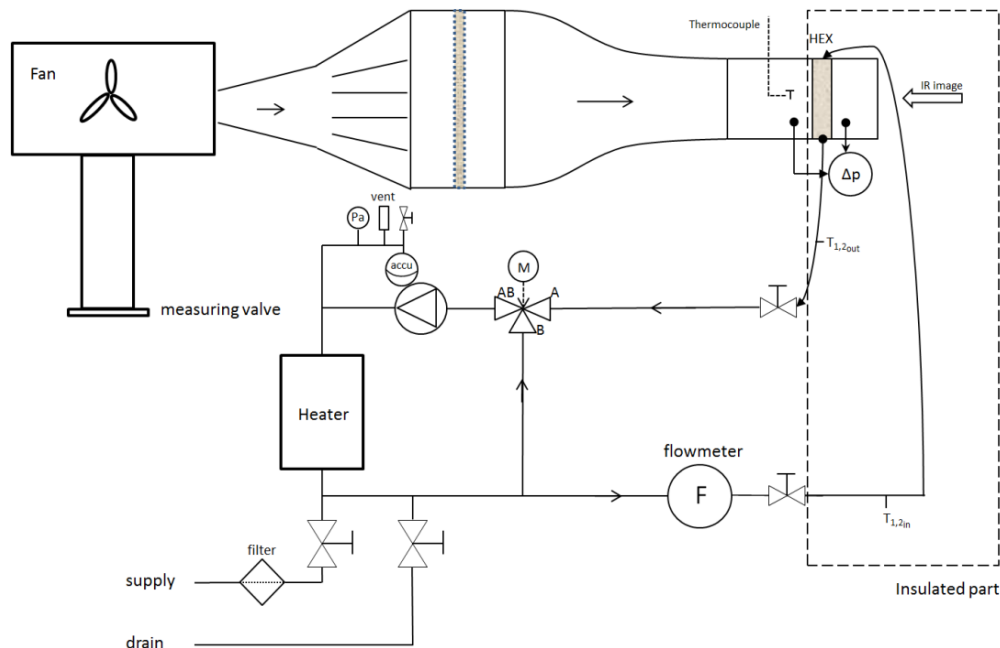
Figure 2 Experimental water- and airside test rig

All water- and airside temperatures are measured with K-type thermocouples (junction diameter of 1 mm), which were calibrated for their specific measuring range using a Druck DBC150 temperature calibrator furnace. The reference temperature is measured with a FLUKE1523 temperature reader with an accuracy of 0.015°C. The uncertainty of the thermocouples is found to be 0.15°C (conservatively). All thermocouples are placed pointing with their tip in the flow direction. The waterside thermocouple measurements are done in two places (to minimize the uncertainty) in a collector just before and after both collectors of the heat exchanger. The inlet air temperature is measured in the center of the test section and is considered to be uniform over the test section.

In order to be able to indicate the quality of the measurements a thorough uncertainty analysis was performed. Standard error propagation rules as described by Moffat [5] were used to determine the total uncertainty (root-sum-square method). The uncertainties on the thermodynamic properties were based on open literature recommendations [6, 7]. In this study all uncertainties are expressed as 95% confidence intervals ($2\,\sigma$).

DATA REDUCTION AND DETERMINATION OF CONSTANTS

Data reduction

$\dot{Q}_{water}$ is calculated through Eq. (1). As the outlet air temperature cannot be measured practically, $\dot{Q}_{air}$ is taken equal to $\dot{Q}_{water}$ (neglecting the heat loss through the insulation). The airside outlet temperature and heat capacity can be determined iteratively by Eq. (2).

$$\dot{Q}_{water} = \dot{m}_{water} \cdot c_{p,water} \cdot (T_{water,in} - T_{water,out}) \quad (1)$$

$$\dot{Q} = \dot{Q}_{avg} = \dot{Q}_{water} = \dot{Q}_{air}$$

$$=> T_{air,out}, c_{p,air} \text{ (iteratively)} \quad (2)$$

The Wilson plot technique [2] is used to determine the airside convective heat transfer coefficient based on experimental data. This technique is based on the separation of the thermal resistance into:

a) Convective heat transfer on waterside (R_{in}) and on airside (R_{ext})
b) Conductive resistance through the aluminium channels (R_{cond})
c) Fouling resistances ($R_{f,in\,\&\,out}$)

$$R_{overall} = \frac{1}{UA} = R_{in} + R_{f,in\,\&\,out} + R_{cond} + R_{ext}, \quad (3)$$

In this equation U is the thermal transmittance and A is the heat transferring surface area. Neglecting the fouling resistances and the conductive resistance, this result in the following expression for the thermal overall resistance (Eq. (4)):

$$R_{overall} = \frac{1}{UA} = \frac{1}{h_{in} \cdot A_{in}} + \frac{1}{\eta \cdot h_{ext} \cdot A_{ext}} \quad (4)$$

As the *F* factor (correction for the flow direction over the heat exchanger) is unknown, the most proper method to determine the overall heat transfer coefficient (*UA*) is through the $\varepsilon - NTU$ method. The cross flow mixed-unmixed equations for the effectiveness are used. The waterside is assumed to be mixed and the airside unmixed [8]. Since there are only 6 fins over the width of the water channel and offset strip fins promote mixing by vortex shedding, the authors approached this as a fully mixed flow across the section of the flat tube. In reality, the flow will in fact not be completely mixed, but the assumption of completely unmixed flow seemed to be less suitable in this case.

$$C_{air} = \dot{m}_{air} \cdot c_{p,air} \quad (5)$$

$$C_{water} = \dot{m}_{water} \cdot c_{p,water} \quad (6)$$

$$C^* = \frac{C_{min}}{C_{max}} \quad (7)$$

$$\dot{q}_{max} = C_{min} \cdot (T_{water,in} - T_{air,in}) \quad (8)$$

$$\dot{q} = C_{water} \cdot (T_{water,in} - T_{water,out}) \quad (9)$$

$$E = \frac{\dot{q}}{\dot{q}_{max}} \quad (10)$$

In case of $C_{air} = C_{min}$,

$$NTU = -\ln\left(\frac{(C^* + \ln(1 - E \cdot C^*))}{C^*}\right) \quad (11)$$

In case of $C_{water} = C_{min}$,

$$NTU = -\frac{\ln(1 + \ln(1 - E) \cdot C^*)}{C^*} \quad (12)$$

Finally:

$$UA = NTU \cdot C_{min} \quad (13)$$

Determination of h_{in}

A correlation from literature is used [9], where an alternative definition for the hydraulic diameter is used (Eq. (14)).

$$D_{h,water} = \frac{4 \cdot s\,h\,l}{2 \cdot (s\,l + h\,l + t\,h) + t\,s} = 0.00265\,m, \quad (14)$$

For this equation the dimensions are taken from Figure 3.

- s: transverse spacing (free flow width) = (3.75-0.3)/1000 m
- h: free flow height = (3-0.3)/1000 m
- t: fin thickness = 0.3/1000 m
- l: fin depth = 1.5/1000 m

$$Re_{D_{h,water}} = \frac{\rho_{water} v_{water} D_{h,water}}{\mu_{water}} \quad (15)$$

$$v_{water} = \frac{\dot{m}_{water}}{\rho_{water} A_{free\,flow,water}} \approx 0.0776 \frac{m}{s} \quad (16)$$

The free flow area in Eq. (16) is calculated based on Figure 3. Every fin is 7.5 mm long, with a height of 3 mm and a fin thickness of 0.3 mm. The width of the channel on waterside is 62.5 mm. There are two spacers present to hold both plates at an equidistant location; both are 7 mm long (as indicated in blue on Figure 3). The number of unit cells of fins is thus approximately 6.5 ($\frac{62.5-2*7}{7.5} = 6.46$). The free flow area is calculated as one unit cell (indicated by the two rectangles colored in red in Figure 3) and multiplied with the number of fins per channel. Finally, to obtain the total free flow area, this number is multiplied with 18 (number of channels on waterside).

$$A_{free\,flow,water} = [[(3.75-0.3)\cdot(3-0.3) + (3.75-0.3)\cdot(3-0.3)]\cdot 6.5]\cdot 18 = 2179.71\ [mm^2], \quad (17)$$

Depending on a critical Reynolds number (Eq. (18)), the Colburn j-factor is determined through Eq. (19) or Eq. (20).

$$Re_{D_{h,water}}{}^* = 257 \cdot \left(\frac{l}{D_{h,water}}\right)^{1.23} \left(\frac{t}{l}\right)^{0.58} D_h \left(t + 1.328 \cdot \left(\frac{Re_{D_{h,water}}}{l\,D_{h,water}}\right)^{-0.5}\right)^{-1} \quad (18)$$
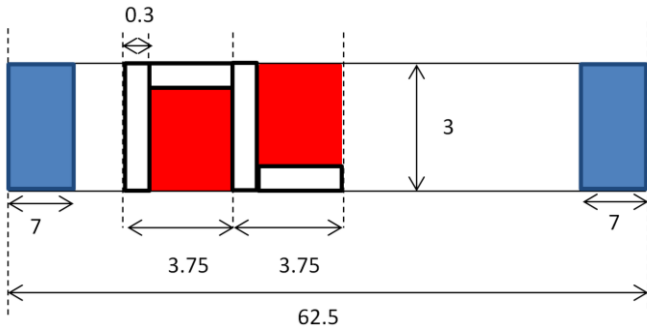
Figure 3 Schematic illustration of the simplifications to calculate A_{flow} (*Figure not to scale – only one unit cell drawn – dimensions are in mm*)

If $Re_{D_{h,water}} < Re_{D_{h,water}}{}^*$

$$j = 0.6522 \left(Re_{D_{h,water}}\right)^{-0.5403} (s/h)^{-0.1541} \cdot (t/l)^{0.1499}(t/s)^{-0.0678} \quad (19)$$

If $Re_{D_{h,water}} \geq Re_{D_{h,water}}{}^*$

$$j = 0.2435 \left(Re_{D_{h,water}}\right)^{-0.4063} (s/h)^{-0.1037} \cdot (t/l)^{0.1955}(t/s)^{-0.1733} \quad (20)$$

Finally, the waterside convection coefficient is calculated through Eq. (21) and (22). A relative uncertainty of 30% is taken on the resulting waterside convection coefficient.

$$St = j/Pr_{water}^{2/3} \quad (21)$$

$$h_{water} = \frac{St\cdot Re_{D_{h,water}}\cdot Pr_{water}\cdot k_{water}}{D_h} \quad (22)$$

Determination of A_{in}

For the determination of A_{in}, the fins are supposed to have no offset in the direction of the water flow. This simplifies the calculation. As there are 18 water channels present with a flow depth of 275 mm and on average 6.5 of those fins, A_{in} is calculated based on the wetted perimeter.

$$A_{in} = wetted\ perimeter\ \cdot 0.275 \cdot 18 = 0.7915\ m^2 \quad (23)$$

The wetted perimeter is calculated based on Figure 4. Again, the calculation is done for one unit cell and multiplied with the number of fins (6.5):

$$wetted\ perimeter = [2\cdot(3.75-0.3) + 2\cdot(3-0.3)]\cdot 2 \cdot 6.5 = 0.1599\ m \quad (24)$$

The absolute uncertainty on the fin length is 0.5 mm, while the uncertainty on the fin thickness is 0.1 mm, on the number of fins 0.5 and on the flow depth of 1 mm. This results in a relative uncertainty on A_{in} of 14%.

Determination of A_{ext}

A_{ext} is determined as the sum of the base plate area, where the hot water flows and the fin area (Eq. (25)).

$$A_{ext} = A_{base\ plate} + A_{fins} = 3.6967\ m^2 \quad (25)$$

As indicated in Figure 4, one wavy fin measures 13 mm and the flow depth on airside is 62.5 mm. This makes (on average) 4.8 wavy fins (as shown in Figure 4(b)). On the other hand, over the width of the heat exchanger (275 mm), there are 55 fins (indicated as triangles in Figure 4(a)): $\frac{275}{5} = 55$. Here the thickness of the fins itself is not taken into account for

simplicity. The area of the base plate is determined through Eq. (26).

$$A_{base\,plate} = 18 \cdot 2 \cdot \frac{(275 \cdot 62.5)}{10^6} = 0.6188 \; m^2 \qquad (26)$$

The area of the fins is determined by multiplying:

- Number of channels at airside: 19 **(1)**
- Number the area of one wavy (indicated in red on Figure 4(b)): $(11.28 \cdot 6.8 \cdot 2) \cdot 2$, taking into account the two legs of the triangle. **(2)**
- Number of sides, top and bottom of the fin: 2 **(3)**
- Number of triangles, as indicated in Figure 4(a): $\frac{275}{5} = 55$ **(4)**
- Number of wavy fins over the airside flow depth: $\frac{62.5}{13} = 4.8$ (on average) **(5)**

$$A_{fins} = (1) \cdot (2) \cdot (3) \cdot (4) \cdot (5) = 3.078 \; m^2 \qquad (27)$$

The uncertainty on A_{ext} is calculated by taking the uncertainty on the number of triangular elements (like in Figure 4(a)) on 1, the uncertainty on length measurements 0.5 mm and on the number of wavy fins in the airside flow depth direction 0.5. This results in a relative uncertainty of 16.7%.

RESULTS AND DISCUSSION

Waterside mass flow rate, *UA* and the heat exchanger's effectiveness (*E*)

First of all, the waterside heat transfer rate ($\dot{Q}_{water}$) is reported (Figure 5). The variation of $\dot{Q}_{water}$ in function of the airside mass flow rate is – as expected – not a linear function, but flattens off. The inlet water temperature is fixed, however, due to ambient conditions, the inlet air temperature varies over the different measuring campaigns. For example, non-uniformity n°3 has a significantly higher heat transfer rate for the first airside velocity set point than the other measurements (see Figure 5). Therefore, the comparison of the three non-uniformities with the uniform case is done by comparing the overall heat transfer conductance (*UA*; see Figure 6).

(a)

(b)
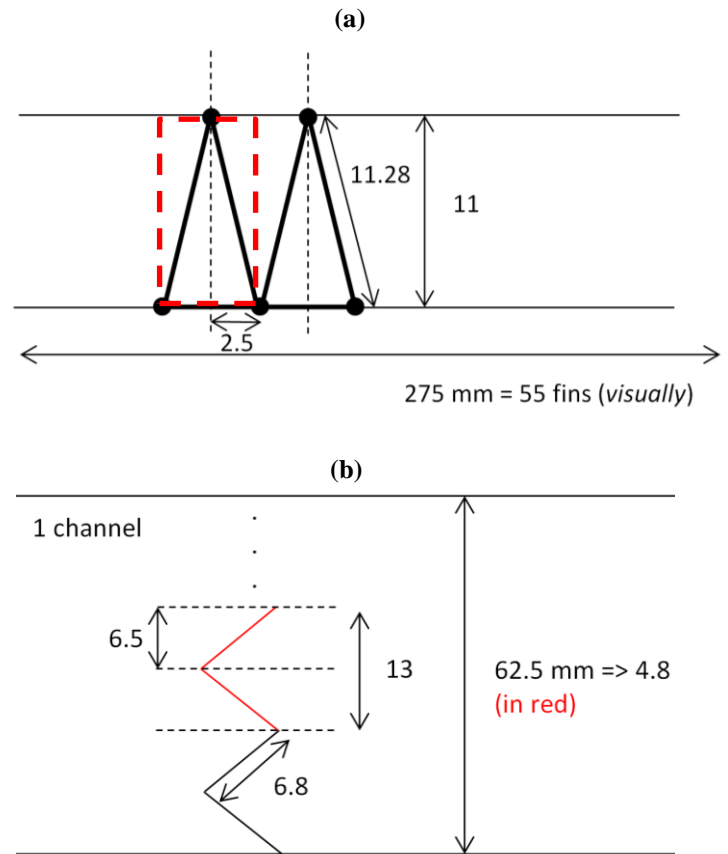
Figure 4 Illustration of the simplifications to determine A_{ext}. (a) front view, (b) top view (*Figure not to scale, dimensions in mm*).
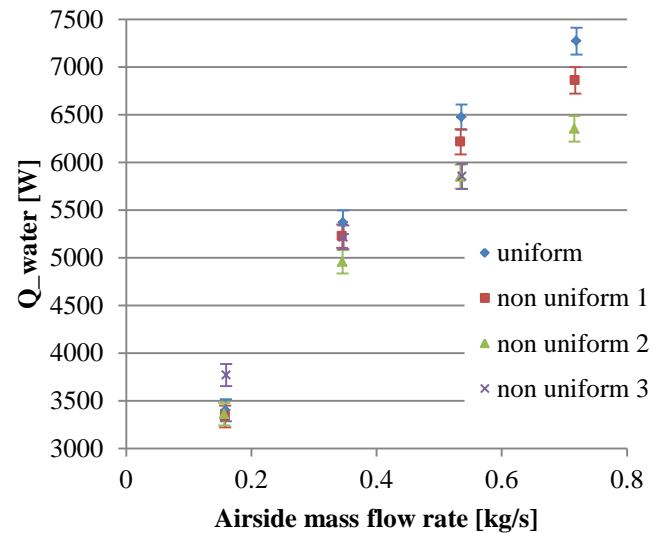
Figure 5 Waterside heat transfer rate ($\dot{Q}_{water}$) in function of the airside mass flow rate for all studied flow conditions

The overall heat transfer conductance (UA) is the product of the overall heat transfer coefficient and the heat exchanger area (Figure 6), where the first term represents the overall thermal resistance to heat transfer from one fluid to another. At the lowest airside mass flow rate, the UA for the second and third non-uniformity is higher than for the uniform case. However, all results at this lowest velocity are within the measurement uncertainty. At higher airside mass flow rates, the uniform case gives the best performance. At the highest velocity, non-uniform case n°2 varies 5.5% (when comparing the average values). However, only the third non-uniformity shows a significant variation from the uniform case: a decrease in UA of 27.3% for the second to last airside mass flow rate. For this last non-uniformity, the pressure drop over het section was so high that last airside velocity set point could not be reached with the current fan unit. The relative uncertainty on the thermal conductance varies from 4.2 to 11%. For the lowest airside mass flow rate, the thermal performance for both uniform and non-uniform cases is the same (within the uncertainty).

For the first two non-uniformities (and at higher airside mass flow rates), the difference in thermal performance in comparison to the uniform case is not high. As only half of the test section is covered, the other half experiences an increase in local airside velocity, approximately by a factor 2. The local convection coefficient will thus also increase on that half of the heat exchanger. However, in the typical empirical correlation $Nu = f(Re, Pr)$, the powers (of Re and Pr) are always smaller than 1. This indicates that the convection coefficient does not increase linearly with velocity. Depending on the evolution of the convection coefficient in function of the airside velocity, the non-uniformity will have limited or larger effect on the thermal performance. As shown in Figure 9, the convection coefficient is approximately linear with the airside velocity for the first two non-uniformities. This results in a limited effect on the heat transfer.

The last non-uniformity is more severe. Although the local airside velocities will be more than tripled over the hole, the increase in convection coefficient will be less. Furthermore, the area over which the air flows is limited. This results in a significant decrease of the heat transfer rate in comparison with the two first non-uniformities.

The heat exchanger effectiveness (the ratio between the actual heat transfer rate and the maximum one; see Figure 7) is declining in function of the airside mass flow rate and has a relative uncertainty between 2.4% and 4.3%. Only the third non-uniformity results in significant lower values for the effectiveness: up to 4.6%-points in comparison with the uniform case for the second to last velocity set point.

Airside convective thermal resistance (R_{ext}) and convection coefficient ($\eta \cdot h$)

The same trends are observed for the airside convective thermal resistance (R_{ext}) and the lumped convection coefficient ($\eta \cdot h = \frac{1}{R_{ext} \cdot A_{ext}}$), as the fin efficiency is difficult to calculate accurately. Non-uniform case n°3 is the only one that flattens off more rapidly. In between non-uniformity 1 and 2, no significant differences are observed. The relative uncertainty

for R_{ext} varies from 7.4% to 11.3% and for the lumped convection coefficient from 13.43% to 16.93%. For the third non-uniformity and the second to last velocity set point the external convective resistance and the lumped convection coefficient are diverging resp. 25.0% and 20.0% with the uniform case.
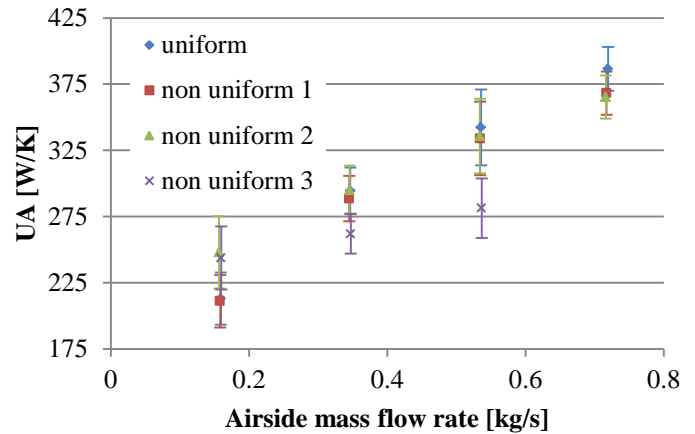

Figure 6 The overall heat transfer coefficient (UA) in function of the airside mass flow rate for all studied flow conditions
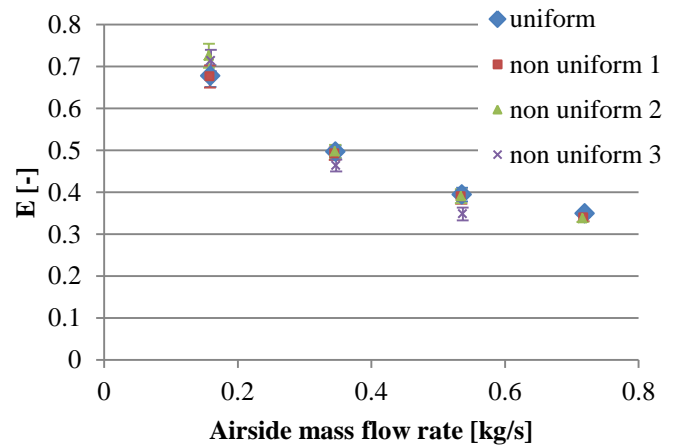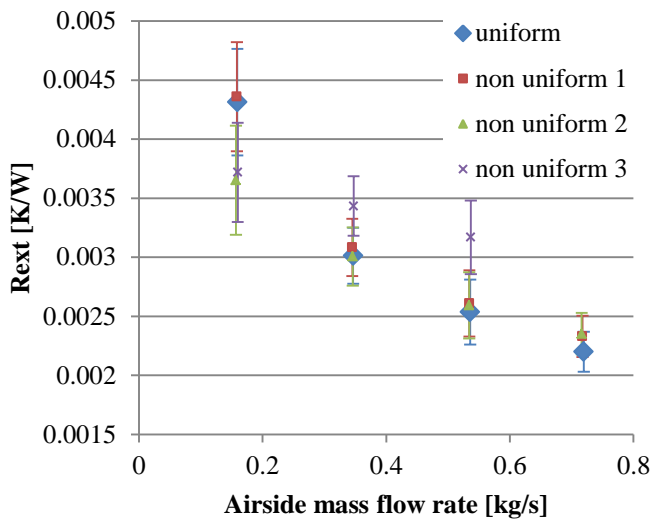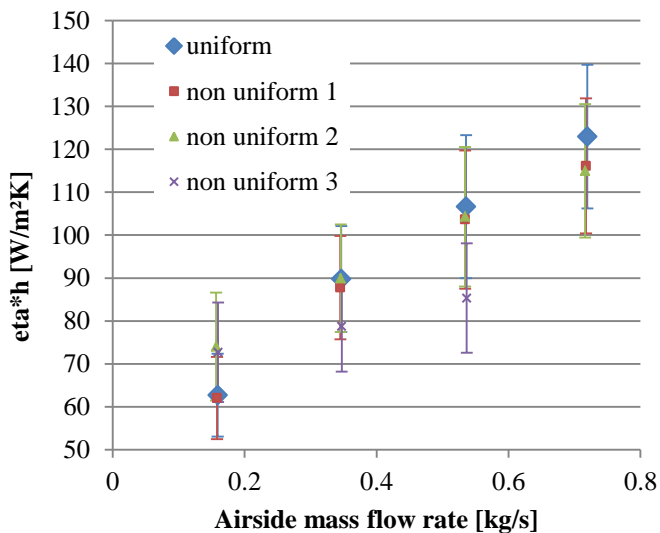

Figure 7 The effectiveness (E) in function of the airside mass flow rate for all studied flow conditions

Figure 8 The external convective resistance (R_{ext}) in function of the airside mass flow rate for all studied flow conditions

Figure 9 The lumped convection coefficient ($\eta \cdot h$) in function of the airside mass flow rate for all studied flow conditions

CONCLUSIONS

In this study, the influence of three non-uniform airside distributions is measured experimentally. It is shown that only severe obstructions (like the one covering over 78.2% of the total flow area; non-uniformity n°3) are causing an effect on the thermal performance. For the other cases, no or little significant effects are observed. This experimental work will be used later to verify a heat exchanger model in CFD software.

REFERENCES

[1] Ameel B., Degroote J., T'Joen C., De Jaeger P., Huisseune H., De Schampheleire S., Vierendeels J., De Paepe M., Optimization of X-shaped louvered fin and tube heat exchangers while maintaining the physical meaning of the performance evaluation criterion, *Applied Thermal Engineering*, Vol. 58, 2013, pp. 136-145

[2] De Schampheleire S., De Jaeger P., Huisseune H., Ameel B., T'Joen C., De Kerpel K., De Paepe M., Thermal hydraulic performance of 10 PPI aluminium foam as alternative for louvered fins in an HVAC heat exchanger, *Applied Thermal Engineering*, Vol. 51, 2013, pp. 371-382.

[3] Beiler M.G., Kröger D.G., Thermal performance reduction in air-cooled heat exchangers due to non-uniform flow and temperature distributions, *Heat Transfer Engineering*, Vol. 17 (1), 1996, pp. 82-92.

[4] T'Joen C., De Paepe M., Vanhee F., Heat exchanger behavior in on uniform flow, *Experimental Heat Transfer*, Vol. 19 (4), 2006, pp. 281-296.

[5] Moffat R.J., Describing the uncertainties in experimental results, *Experimental Thermal Fluid Science*, Vol. 17 (3), 1988, pp. 3-17

[6] Kadoya K., Matsunaga N., Nagashima A., Viscosity and thermal conductivity of dry air in the gaseous phase, *Journal of Physical Chemical Ref. Data*, Vol. 14, 1985, pp. 947-970

[7] Wagner W., Prub A., The IAPWS formulation 1995 for the thermodynamic properties of ordinary water substance for general and scientific use, *Journal of Physical Chemical Ref. Data*, Vol. 31, 2002, pp. 387-535

[8] Shah R.K., Sekulic D.P., *Fundamentals of Heat Exchanger Design*, Hoboken, New Jersey, 2003, John Wiley & Sons

[9] Teruel M.H., Nakaskima C.Y., Paglione P., Rectangular offset strip-fin heat exchanger lumped parameters dynamic model, *Prod. of 3rd CTA-DLR Workshop on data analysis & Fight control*, S.J. Campos, Brazil, 2009. Online available on: http://www.cta-dlr2009.ita.br/Proceedings/PDF/59420.pdf